Supplementary Information

Deciphering and Constructing the Quorum Sensing Language "Interpreter" Ecosystem for Microbial Community

Shengbo Wu[1,2,†], Hong Zhang[1,†], Yongsheng Zhou[1,†], Chengyang Xu[1], Boxin Yuan[1], Haijiao Wang[1], Danlei Chen[1,2], Chunjiang Liu[1,2,3], Qinggele Caiyin[1,2], Hao Wu[1,2], Aidong Yang[4], Kun Zhao[5,6*], Jianjun Qiao[1,2,7,8*]

[1]School of Chemical Engineering and Technology, Tianjin University, Tianjin, 300072, China
[2]Zhejiang Shaoxing Research Institute of Tianjin University, Shaoxing, 312300, China
[3]State Key Laboratory of Chemical Engineering, Tianjin University, Tianjin 300072, China
[4]Department of Engineering Science, University of Oxford, Oxford OX1 3PJ, UK
[5]Sichuan Provincial People's Hospital, University of Electronic Science and Technology of China, Chengdu, Sichuan 610054, China
[6]Institute of Fundamental and Frontier Sciences, University of Electronic Science and Technology of China, Chengdu, Sichuan 610054, China
[7]Key Laboratory of Systems Bioengineering, Ministry of Education (Tianjin University), Tianjin, 300072, China
[8]Frontiers Science Center for Synthetic Biology (Ministry of Education), Tianjin University, Tianjin, 300072, China

†These authors contributed equally to this work.

*Correspondence and requests for materials should be addressed to

Kun Zhao (email: kzhao@uestc.edu.cn)

Jianjun Qiao (email: jianjunq@tju.edu.cn)

Contents

1. Research framework

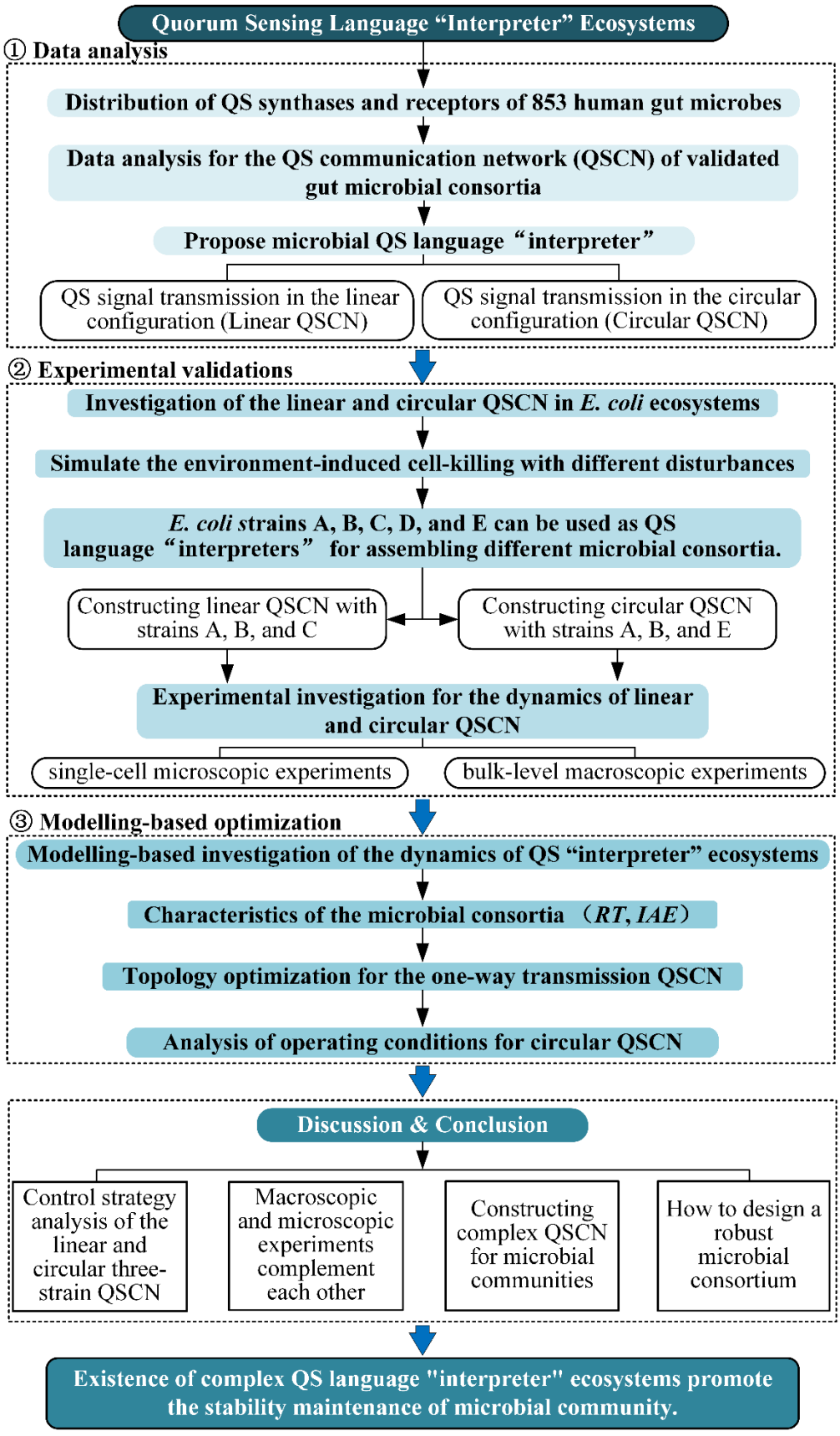

Supplementary Fig. 1. A diagram illustrating the research framework of the study.

2. Supplementary figures and tables for experiments

Supplementary Table 1. Reagents and instruments used in this study.

Reagents	Source
Phanta Super Fidelityenzyme	Vazyme Biotech (China)
Restriction endonucleases	New England Biolabs
T4 DNA ligase	New England Biolabs
TIANprep Mini Plasmid Kit	Tiangen Biotech (China)
TIANgel Midi Purification Kit	Tiangen Biotech (China)
TIANquick Midi Purification Kit	Tiangen Biotech (China)
Universal DNA Purification Kit	Tiangen Biotech (China)
pEASY®-Basic Seamless Cloning and Assembly Kit	TransGen Biotech (China)
Antibiotics and other reagents	Dingguo Biotech (China)
Instruments	**Source**
TGL-16G centrifuge	Shanghai Anting Scientific Instrument factory
Benchtop Centrifuge	Thermo Scientific
UV/VIS spectrophotometer	Beijing Purkinje General Instrument Co., Ltd
ELIASA	Molecular Devices
PCR-Cycler	Thermo Scientific
QE-1 Shaker	Tianjin Honour lnstrument Co., Ltd
FE20 – FiveEasy Plus™ pH	METTLER-TOLEDO
Nucleic Acid Electrophoresis	Liuyi Biotech (China)
Leica DMIRB	Leica
UV gel imaging system	Baygene Biotech
-80℃ ultra low temperature refrigerator	Thermo Scientific
Eporator Electroporation	Eppendorf
0.2cm Electric rotor	Eppendorf
SW—CL—1G Clean Bench	Suzhou Purification Equipment Co., Ltd

Supplementary Table 2. Strains used in this study.

Strains	Characteristics	Sources
E.coli *Trans*DB3.1	F-*gyr*A462 *end*A1Δ(*sr1-rec*A)*mcr*B *mrr* *hsd*S20(r_B^-,m_B^-)*sup*E44*ara*-14 *gal*K2 *lac*Y1 *pro*A2 rpsL20(Sm^R) *xyl*-5λ-*leumtl*1	TransGen Biotech
L31SR-P	pCL-P_{esaR-P}-*mkate*+pCOLA-P_{esaS}-*gfp*	[1]
Strain A	*E.coli* with petduet-1-A & p15AT-A	This study
Strain B	*E.coli* with petduet-1-B & p15AT-B	This study
Strain C	*E.coli* with petduet-1-C2 & p15AT-CM	This study
Strain D	*E.coli* with petduet-1-C3 & p15AT-CM	This study
Strain E	*E.coli* with petduet-1-C1 & p15AT-CM	This study

Supplementary Table 3. Plasmids used in this study.

Plasmids	Gene cluster	Sources
petduet-1	petduet-1 ori； amp^R	[2]
p15AT	p15A ori with *ccdB;* Cm^R	This study
p15AT-CM	p15AT with Δ*ccdB*	This study
p15AT-A	p15A with *Plac-ccdB-*P_{AR}*-bfp*	This study
p15AT-B	p15A with *Para-ccdB-Pleteo-gfp*	This study
petduet-1-A	Petduet-1 with *luxI-rpaR-Prpa-ccdA*	This study
petduet-1-B	Petduet-1 with *lasI-luxR-Plux-ccdA*	This study
petduet-1-C1	Petduet-1 with *RpaI-lasR-Plas-citA-*P_{AR}*-rfp*	This study
petduet-1-C2	Petduet-1-*lasR-RpaI-*P_{AR}*-rfp*	This study
petduet-1-C3	Petduet-1 with *RpaI-EsaRI70V-PesaS-ccdA-PesaR-ccdB-*P_{AR}*-rfp*	This study

Supplementary Table 4. Primers used in this study.

Primers	Sequences (5'-3')
Petduet-1-general-F	ggccacgatgcgtcc
Petduet-1-general-R	ctgcgctagtagacgagtcc
p15AT-YZ-F1	agtgatcttatttcattatggtg
p15AT-YZ-R1	tcaggtgctacatttgaagagata
p15AT-YZ-F2	gaagcagcccagtagtaggttg
p15AT-YZ-R2	gttttatttgatgcctggaga

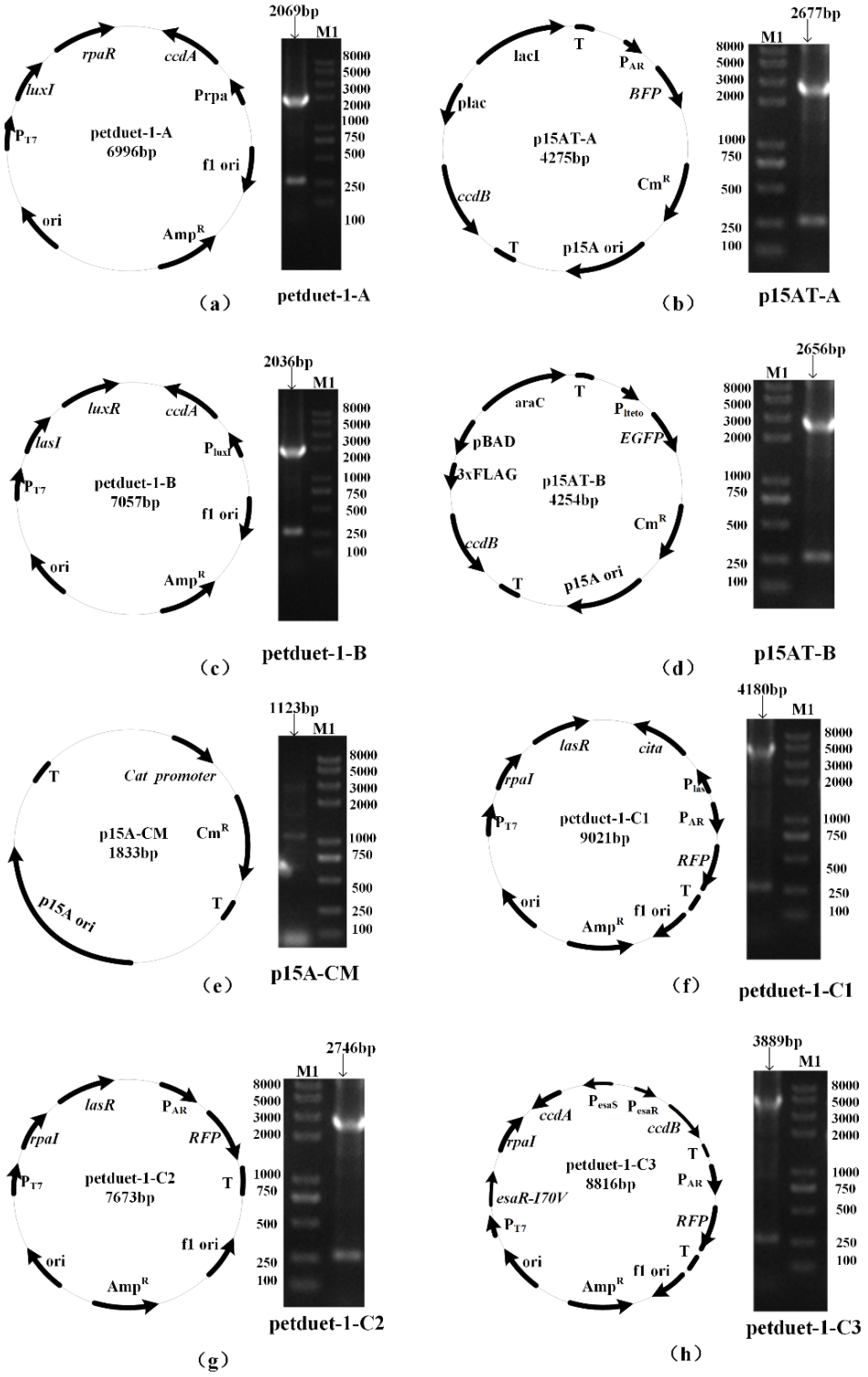

Supplementary Fig.2. Plasmid maps and verification electrophoresis for various plasmids.

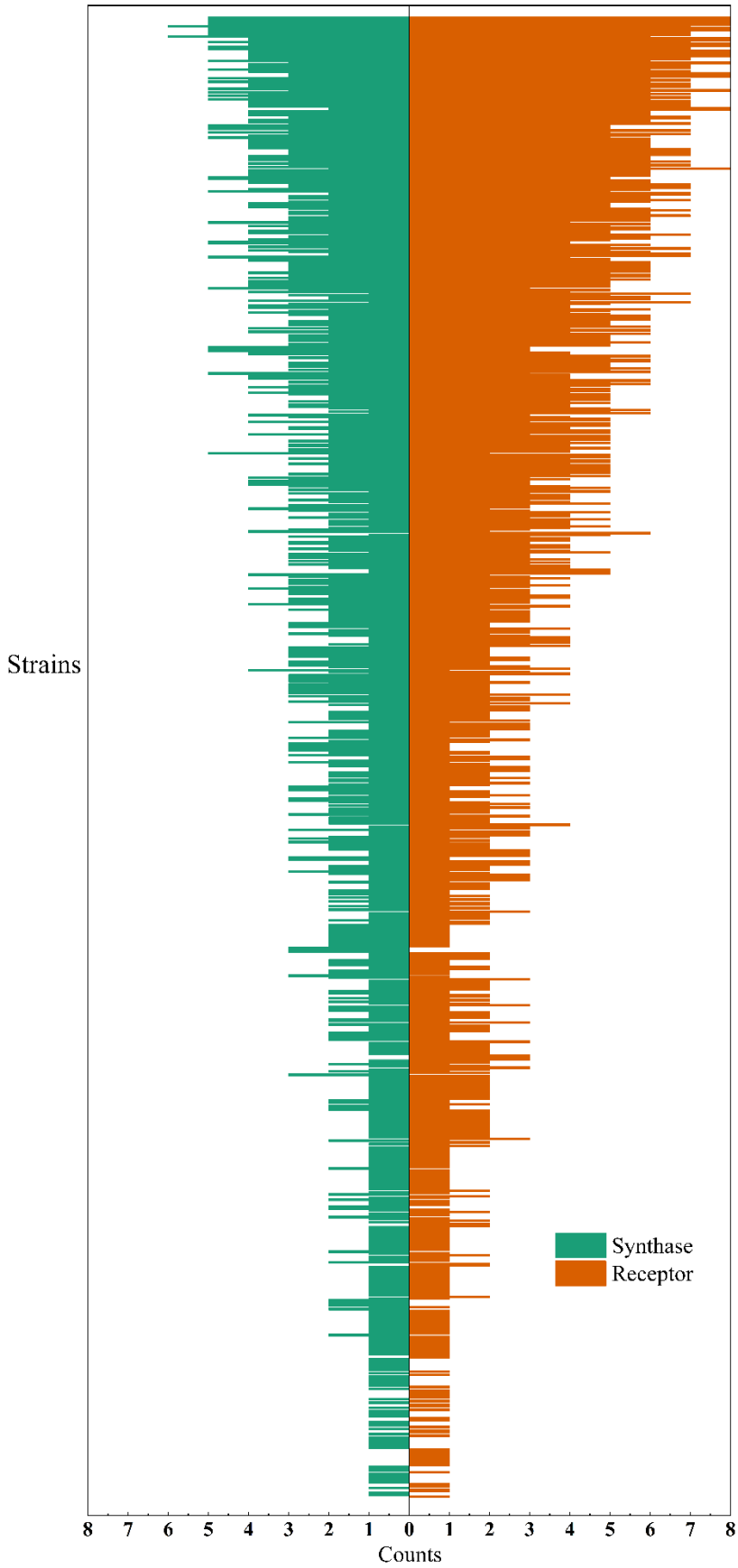

Supplementary Fig. 3. Distribution of the QS synthases and receptors of 853 human gut microbes.

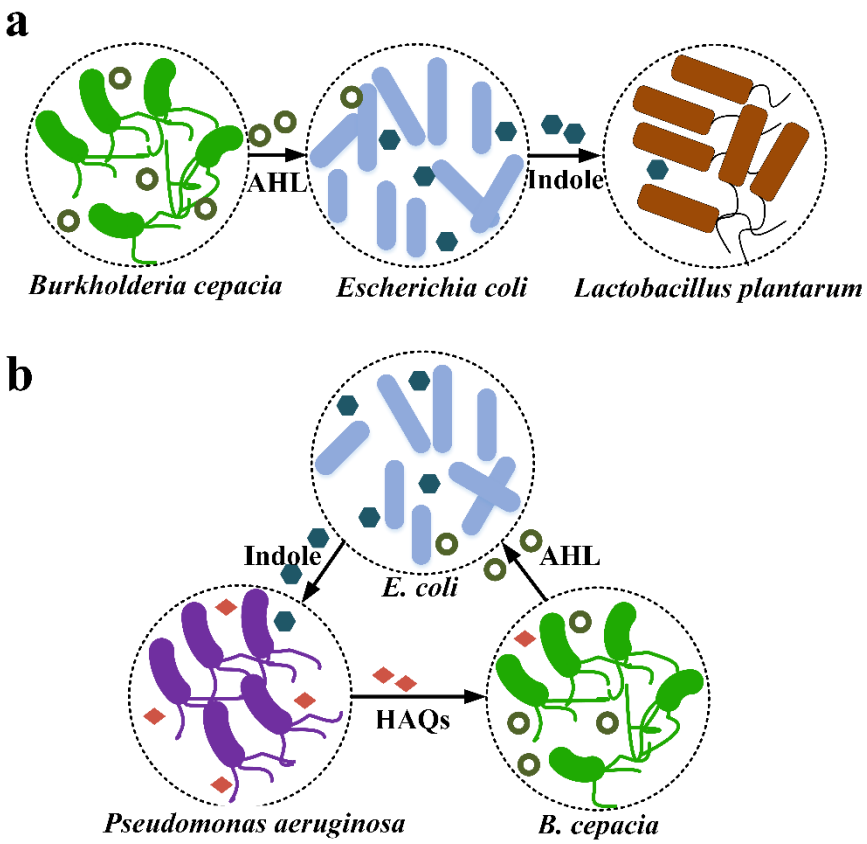

Supplementary Fig. 4. Diagram of potential QS-based "interpreter" ecosystems in natural communities. a. Diagram of a linear microbial ecosystem that communicated based on acyl-homoserine lactones (AHL) and indole. b. Diagram of a circular ecosystem that communicated based on AHL, indole, and 4-hydroxy-2-alkylquinolines (HAQs).

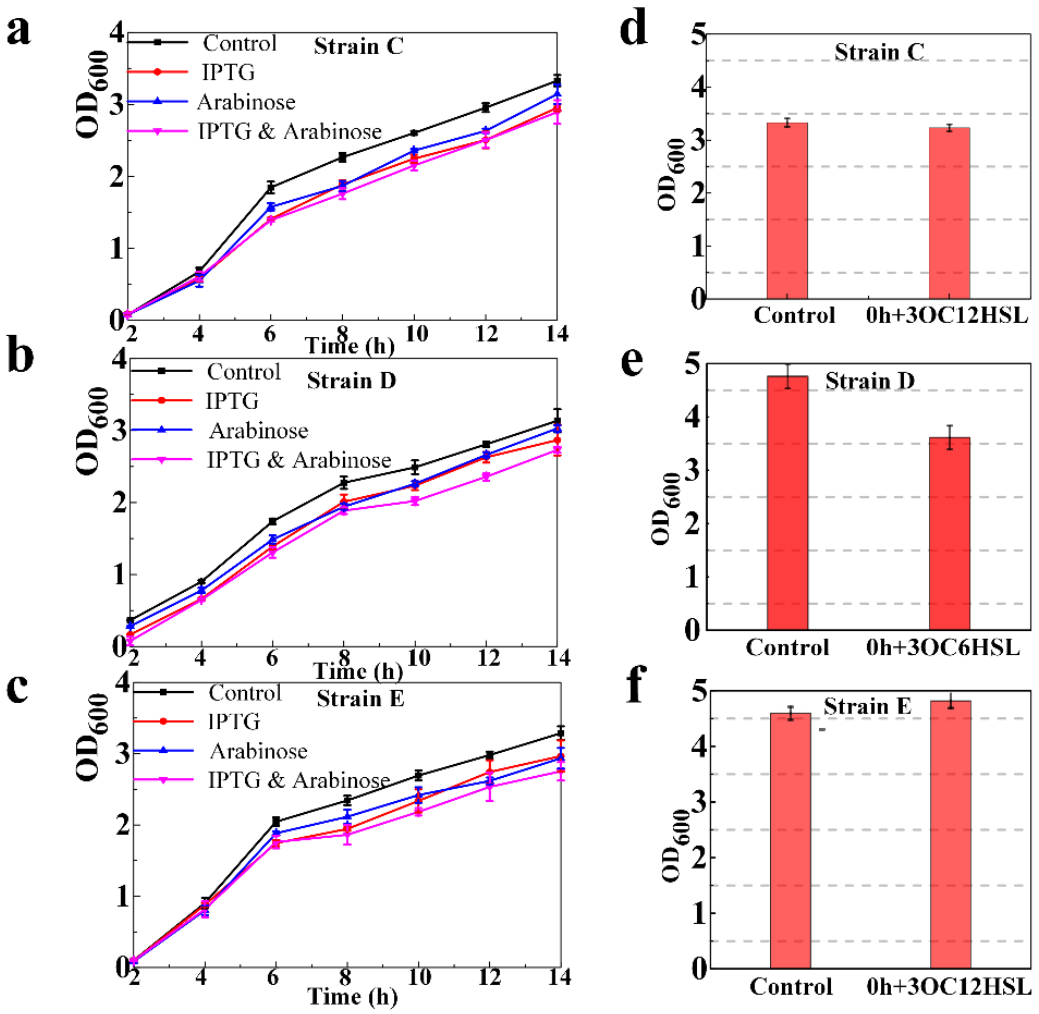

Supplementary Fig. 5. Experimental results for strain C, D, and E. a-c. either IPTG or arabinose will not affect much the cell growth of strains C, D, and E. d. The addition of QS signals has little effect on the cell growth of strain C, as there are no heterologous proteins that promote or inhibit its cell growth. e. the addition of QS signal led to the reduction of the density of strain D. f. Strain D has two *esa* promoters, P_{esaS} and P_{esaR}. When the concentration of 3OC6HSL is very low, P_{esaS} will be turned on, but it will be gradually inhibited with the increase of 3OC6HSL concentration, which will lead to a decrease in CcdA expression and the activation of CcdB promoted by P_{esaR}. Thus, for strain D, when 3OC6HSL is added at the beginning, a reduced cell density at 24h would be obtained. We have also introduced a citrate synthase (*citA*) in strain E to enhance the TCA cycle and accelerate cell growth, which is induced by the native promoter from *las* QS system (P_{las}). Due to the non-rigorousness of P_{las}, there could be a certain degree of background expression of CitA in the control case, which results in a slightly higher cell density of strain E with the addition of 3OC12HSL than the control case.

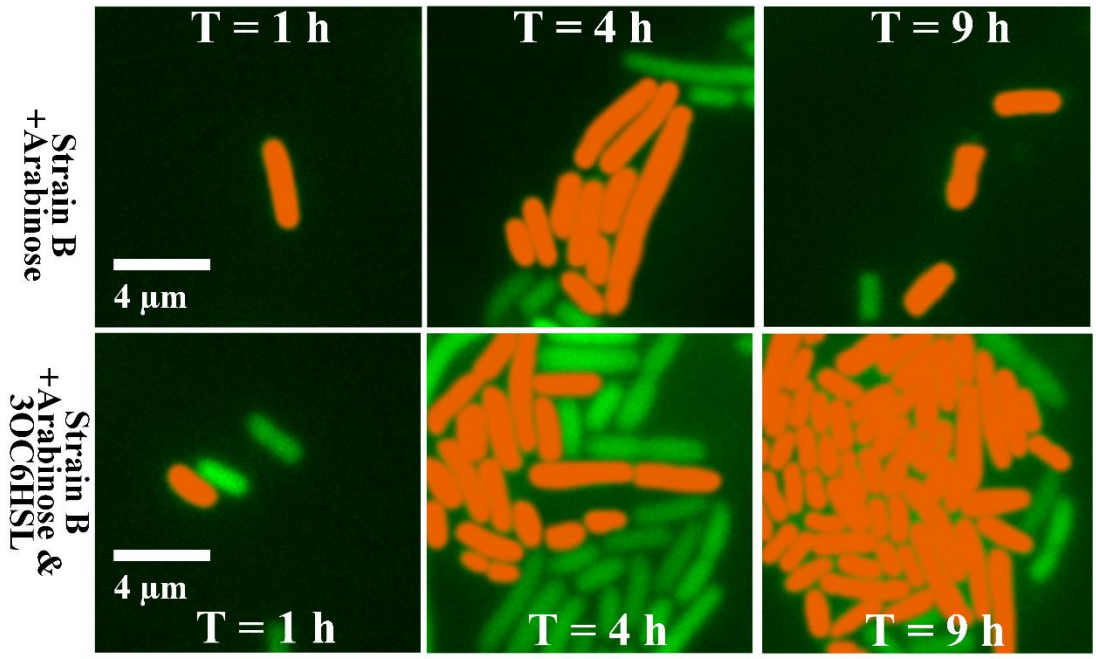

Supplementary Fig. 6. Microscopic imaging of strain B under an arabinose-included plate with or without 3OC6HSL. The cells colored by brown at T = 4h and T = 9h are progenies of the brown-colored cell at T = 1h.

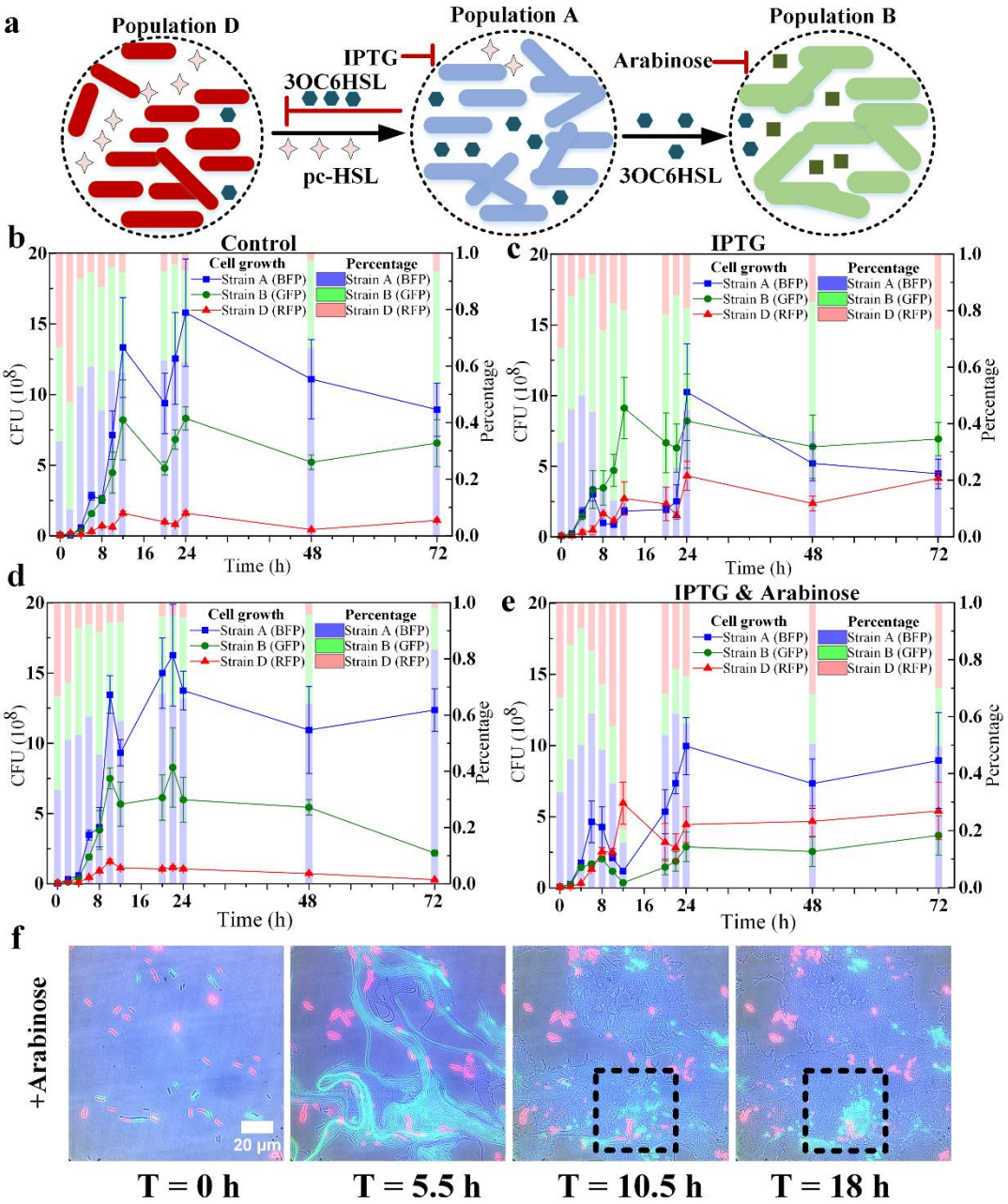

Supplementary Fig. 7. Experimental results for a linear QS-based consortium with an inhibition inter-species interaction. a. Schematic diagram of the QS-based communications in the linear consortium. b-e. The cell growth (line) and corresponding population percentage(column) of each strain in the consortium for cases of without inducers (as a control) (b), with IPTG (c), with arabinose (d), and with both two inducers (e). f. Microscopic experimental results for the case of arabinose addition.

For the cases of the control and arabinose addition where the growth of strain A was not inhibited, the cell density of strain A was the highest, which then suppressed the growth of strain D and resulted in a very low cell percentage. The final ratio of the three strains (D:A:B) at 72 h reached 1:8.17:6 for the control and 1:42.4:7.5 under arabinose addition. In contrast, under IPTG addition, where IPTG could induce CcdB expression in strain A, the cell percentage of strain A was considerably reduced; thus, the cell percentage of strain D was increased compared to the cases in Supplementary Fig. 6b and 6d. The final ratio of the three strains (D:A:B) at 72 h was 1:1.08:1.67 under IPTG addition case and 1:1.66:0.68 under both IPTG and arabinose addition.

Supplementary Table 5. Total cell-density differences of the linear and circular QS signal transmission.

	IPTG addition			Arabinose addition			IPTG & arabinose addition		
QSCN	Linear	Circular	*P* value	Linear	Circular	*P* value	Linear	Circular	*P* value
BFP strain (A)	38.03	17.63	** P=0.0015< 0.01	6.98	5.87	P=0.372> 0.05	18.66	15.20	* P=0.036< 0.05
	38.22	14.97		7.81	9.29		22.39	11.85	
	36.45	20.49		10.20	9.97		21.42	18.54	
Average	**37.57**	**17.70**		**8.33**	**7.83**		**20.82**	**16.86**	
GFP strain (B)	17.21	5.83	** P=0.0004< 0.01	14.89	12.87	P=0.094> 0.05	15.23	11.49	** P=0.005< 0.01
	19.35	5.79		17.36	11.94		13.95	11.81	
	19.95	7.21		17.66	16.67		15.20	10.91	
Average	**18.84**	**6.27**		**16.64**	**13.83**		**14.80**	**9.78**	
RFP strain (C/E)	18.33	10.06	* P=0.0104 < 0.05	14.68	6.01	** P=0.006< 0.01	15.84	12.17	** P=0.008< 0.01
	17.86	10.90		12.44	3.79		14.60	10.70	
	14.60	12.89		17.69	4.49		14.37	9.07	
Average	**16.93**	**11.28**		**14.94**	**4.76**		**14.94**	**10.63**	

Note that the unit is CFU (10^8)

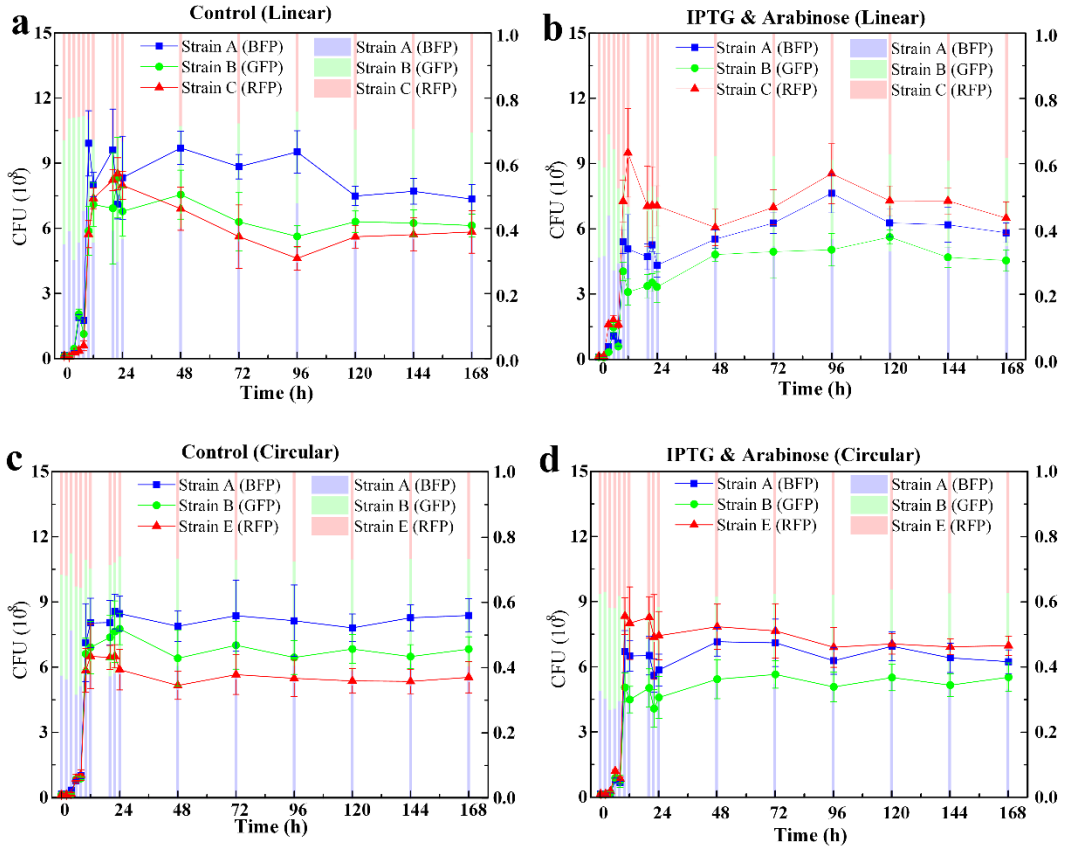

Supplementary Fig. 8. One-week experimental results for a linear (upper) and circular QS-based consortium (downer) with the addition of IPTG and arabinose.

Supplementary Table 6. Total cell density difference of the linear and circular QS signal transmission.

Disturbance	IPTG & arabinose addition		Statistical significance
Configurations	Linear	Circular	*P*
Difference of BFP strain (A)	30.81	17.32	*, 0.0165<0.05
	29.98	20.30	
	39.58	21.22	
Difference of GFP strain (B)	28.21	22.39	**, 0.0015<0.01
	26.65	20.14	
	29.29	21.56	
Difference of RFP strain (C/E)	28.38	18.23	*, 0.0244<0.05
	26.17	19.81	
	22.68	20.93	

Note that the unit is CFU (10^8)

3. Modeling-based investigation

3.1 Mathematical modelling development

The complete ODE modelling development for QS-based circular-interaction consortium is listed in the following equations S1-13. Three QS systems commonly used in recent studies (*lux* QS [3], *las* QS [4], and *rpa* QS [5]) were investigated in modelling development. The QS model construction were based on our previous work [6]. Based on the previous QS-relevant work [5, 7-9], we also obtained some important parameters, such as the basic QS-regulated growth rates (γ_A, γ_B and γ_E), calibrated in this work from our experimental results. As illustrated in Supplementary Fig. 9a, simulation results agreed well with the experimental data. It formed a basis for the dynamic simulation of the circular microbiota with ten-percent (±10%) or fifty-percent (±50%) disturbances imposed on strain A (BFP strain), strain B (GFP strain), or strain E (RFP strain), as well as the analysis of operating conditions, such as initial inoculum ratio and dilution rate, for the circular-interaction consortium and topology optimization on the one-way control consortia. We listed ODE equations in cocultivation of the strain A, strain B and strain E for cell growth and QS mechanisms as follows.

Cell growth for strain A, strain B, and strain E:

$$\frac{dC_A}{dt} = g_A \cdot C_A \cdot \left(1 - \frac{C_A+C_B+C_E}{C_m}\right) + \frac{A_3^2}{{A_{c3}}^2+A_3^2} \cdot x \cdot \gamma_A \cdot C_A - D \cdot C_A \quad \text{(S1)}$$

$$\frac{dC_B}{dt} = g_B \cdot C_B \cdot \left(1 - \frac{C_A+C_B+C_E}{C_m}\right) + \frac{A_1^2}{{A_{c1}}^2+A_1^2} \cdot y \cdot \gamma_B \cdot C_B - D \cdot C_B \quad \text{(S2)}$$

$$\frac{dC_E}{dt} = g_E \cdot C_E \cdot \left(1 - \frac{C_A+C_B+C_E}{C_m}\right) + \frac{A_2^2}{{A_{c2}}^2+A_2^2} \cdot z \cdot \gamma_E \cdot C_E - D \cdot C_E \quad \text{(S3)}$$

where the g_A, g_B, g_E are the growth rate of strains A, B, and E, respectively. x, y, and z are the constants for the extra growth rate of strain A contributed by strain E, the constant for the extra growth rate of strain B contributed by strain A, and the constant for the extra growth rate of strain E contributed by strain B, respectively. The above three constants are used to illustrate the interaction types among different strains, such as inhibition (-1), no interaction (0), or promotion (1). γ_A, γ_B, and γ_E are basic QS-regulated growth rate of strains A, B, and E, respectively. More details for parameters descriptions and values are listed in Supplementary Table 7.

In the following equations, we utilized the number "1", "2", "3" to represent the 3OC6HSL, 3OC12HSL, and pc-HSL, respectively. There are some reasonable assumptions for our mathematical modelling as follows.

a. Three QS systems (*lux*, *las*, and *rpa*) are orthogonal[10] for the QS signal receiving.
b. The value of the Hill coefficient for the concentration of AHL is set to be 2.[7]
c. Based on the sensitive analysis for different QS parameters in our previous study[6, 11], the other parameters for the three QS systems in the consortium remain the same except the four parameters (α_q, α_q^*, A_c, and γ_{AHL}).

Concentration of the pc-HSL from strain E:

$$\frac{dA_3}{dt} = \left(\alpha_{q3} + \alpha_{q3}^* \cdot \frac{A_3^2}{A_{c3}^2+A_3^2}\right) \cdot C_3 - (\gamma_{A3} + D) \cdot A_3 - 2\rho_1 \cdot A_3^2 \cdot R_1^2 + 2\gamma_{AR1} \cdot AR_1 \quad \text{(S4)}$$

Concentration of the RpaR (QS receptor of the pc-HSL) in strain A:

$$\frac{dR_1}{dt} = v_{R1} \cdot C_1 - (\gamma_{R1} + D) \cdot R_1 - 2\rho_{R1} \cdot R_1^2 \cdot A_3^2 + 2\gamma_{AR1} \cdot AR_1 \quad \text{(S5)}$$

Concentration of the complex of RpaR and pc-HSL in strain A:

$$\frac{dAR_1}{dt} = \rho_{R1} \cdot R_1^2 \cdot A_3^2 - (\gamma_{AR1} + D) \cdot AR_1 \quad \text{(S6)}$$

Concentration of the 3OC6HSL from strain A:

$$\frac{dA_1}{dt} = \left(\alpha_{q1} + \alpha_{q1}^{*} \cdot \frac{A_1^2}{A_{c1}^2 + A_1^2}\right) \cdot C_1 - (\gamma_{A1} + D) \cdot A_1 - 2\rho_2 \cdot A_1^2 \cdot R_2^2 + 2\gamma_{AR2} \cdot AR_2 \quad \text{(S7)}$$

Concentration of the LuxR (QS receptor of the 3OC6HSL) in strain B:

$$\frac{dR_2}{dt} = v_{R2} \cdot C_2 - (\gamma_{R2} + D) \cdot R_2 - 2\rho_{R2} \cdot R_2^2 \cdot A_1^2 + 2\gamma_{\mathrm{AR2}} \cdot AR_2 \quad \text{(S8)}$$

Concentration of the complex of LuxR and 3OC6HSL in strain B:

$$\frac{dAR_2}{dt} = \rho_{R2} \cdot R_2^2 \cdot A_1^2 - (\gamma_{\mathrm{AR2}} + D) \cdot AR_2 \quad \text{(S9)}$$

Concentration of the 3OC12HSL from strain B:

$$\frac{dA_2}{dt} = \left(\alpha_{q2} + \alpha_{q2}^{*} \cdot \frac{A_2^2}{A_{c2}^2 + A_2^2}\right) \cdot C_2 - (\gamma_{A2} + D) \cdot A_2 - 2\rho_3 \cdot A_2^2 \cdot R_3^2 + 2\gamma_{\mathrm{AR3}} \cdot AR_3 \quad \text{(S10)}$$

Concentration of the LasR (QS receptor of the 3OC12HSL) in strain E:

$$\frac{dR_3}{dt} = v_{R3} \cdot C_3 - (\gamma_{R3} + D) \cdot R_3 - 2\rho_{R3} \cdot R_3^2 \cdot A_2^2 + 2\gamma_{\mathrm{AR3}} \cdot AR_3 \quad \text{(S11)}$$

Concentration of the complex of LasR and 3OC12HSL in strain E:

$$\frac{dAR_3}{dt} = \rho_{R3} \cdot R_3^2 \cdot A_2^2 - (\gamma_{\mathrm{AR3}} + D) \cdot AR_3 \quad \text{(S12)}$$

Dilution rate (D) is calculated from Balagadde et al.[7]:

$$D = -ln(1 - F)/T \quad \text{(S13)}$$

where F is the fraction of dilution and T represents the time interval between each dilution event. where the other parameters descriptions and values are listed in Supplementary Table 6 in the supplementary information. Note that the 100 ml medium was diluted every 12 h and 10 ml was added (the corresponding D was 0.01 h^{-1} approximately). For the sensitivity analysis on D, the 100 ml medium were diluted every 12 h with the corresponding D being about 0.043 h^{-1}, 0.076 h^{-1}, and 0.134 h^{-1}, respectively.

Supplementary Table 7. Values of parameters for the circular-promotion consortium

Parameters	Description	Value	Unit	Data sources
g_A	Growth rate of the strain A	0.77	h^{-1}	This study
g_B	Growth rate of the strain B	0.76	h^{-1}	This study
g_E	Growth rate of the strain E	0.74	h^{-1}	This study
γ_A	Growth promotion rate from CcdA for the resistance for CcdB in strain A	0.01	h^{-1}	This study
γ_B	Growth promotion rate from CcdA for the resistance for CcdB in strain B	0.01	h^{-1}	This study
γ_E	Growth promotion rate from CitA	0.01	h^{-1}	This study
D	Dilution rate in strain E	0.01	h^{-1}	This study
C_m	Carrying capacity for cell growth	20.0	CFU/mL (10^6)	This study
α_{q1}	Basal production rate of 3OC6HSL (*lux* AHL)	0.4	nM ml hr^{-1}	[5]
α_{q1}^*	Maximum production rate of the *lux* AHL	8	nM ml hr^{-1}	[5]
A_{c1}	Concentration of AHL necessary to half-maximally active P_{luxI} promoter	1	nM	[5]
γ_{A1}	Decay rate constant of *lux* AHL in the cell	1	h^{-1}	[5]
α_{q2}	Basal production rate of 3OC12HSL (*las* AHL)	0.5	nM ml hr^{-1}	Est. from [5, 9]
α_{q2}^*	Maximum production rate of the *las* AHL	25	nM ml hr^{-1}	Est. from [5, 9]
A_{c2}	Concentration of AHL necessary to half-maximally active P_{las} promoter	0.26	nM	Est. from [5, 9]
γ_{A2}	Decay rate constant of *las* AHL in the cell	0.8	h^{-1}	Est. from [5, 9]
α_{q3}	Basal production rate of pc-HSL (*rpa* AHL)	0.72	nM ml hr^{-1}	Est. from [5, 9]
α_{q3}^*	Maximum production rate of the *rpa* AHL	7	nM ml hr^{-1}	Est. from [5, 9]
A_{c3}	Concentration of AHL necessary to half-maximally active P_{rpa} promoter	0.1	nM	Est. from [5, 9]
γ_{A3}	Decay rate constant of *rpa* AHL in the cell	1.2	h^{-1}	Est. from [5, 9]
ρ	QS complex dimerization constant	0.5	\	[5, 12]
ν_R	Production rate of QS receptor	1	h^{-1}	[5, 12]
γ_R	Decay rate constant of receptor in the cell	0.1	h^{-1}	[5, 12]
γ_{AR}	Decay rate constant of complex in the cell	0.023	h^{-1}	[5, 12]

3.2 The employment of RT and IAE

Quantitatively, we employed two parameters from control theory[13], the response time (RT) and the integral of absolute error (IAE), to characterize the dynamics of the QS-regulated circular-interaction microbial consortium. The constructed model without disturbance (Supplementary Fig. 9a) would serve as a basis for combining other relevant model components to simulate new cases.

Results show that there is almost no difference in RT between the cases with +10% and–10% (+50% and–50%) cell density disturbances (Supplementary Fig. 10). However, RT of 50% disturbance is typically 2-3 h longer than that of 10% disturbance (Supplementary Fig. 11). The circular three-strain system could remain relatively stable for 10% change (Supplementary Fig. 9e) with a three-strain ratio that fluctuate slightly around 1:1:1. The system could still reach to a stable state for 50% change, but with a three-strain ratio that varies and can differ greatly from 1:1:1(Supplementary Fig. 9f). The results of IAE (ranging from 20 h to 72 h) analysis further demonstrate that among three strains, the stability of the system is affected most by the disturbance of strain A, followed by the disturbance of strain B and the disturbance of strain E has the least effect (Supplementary Fig. 9g and 9h).

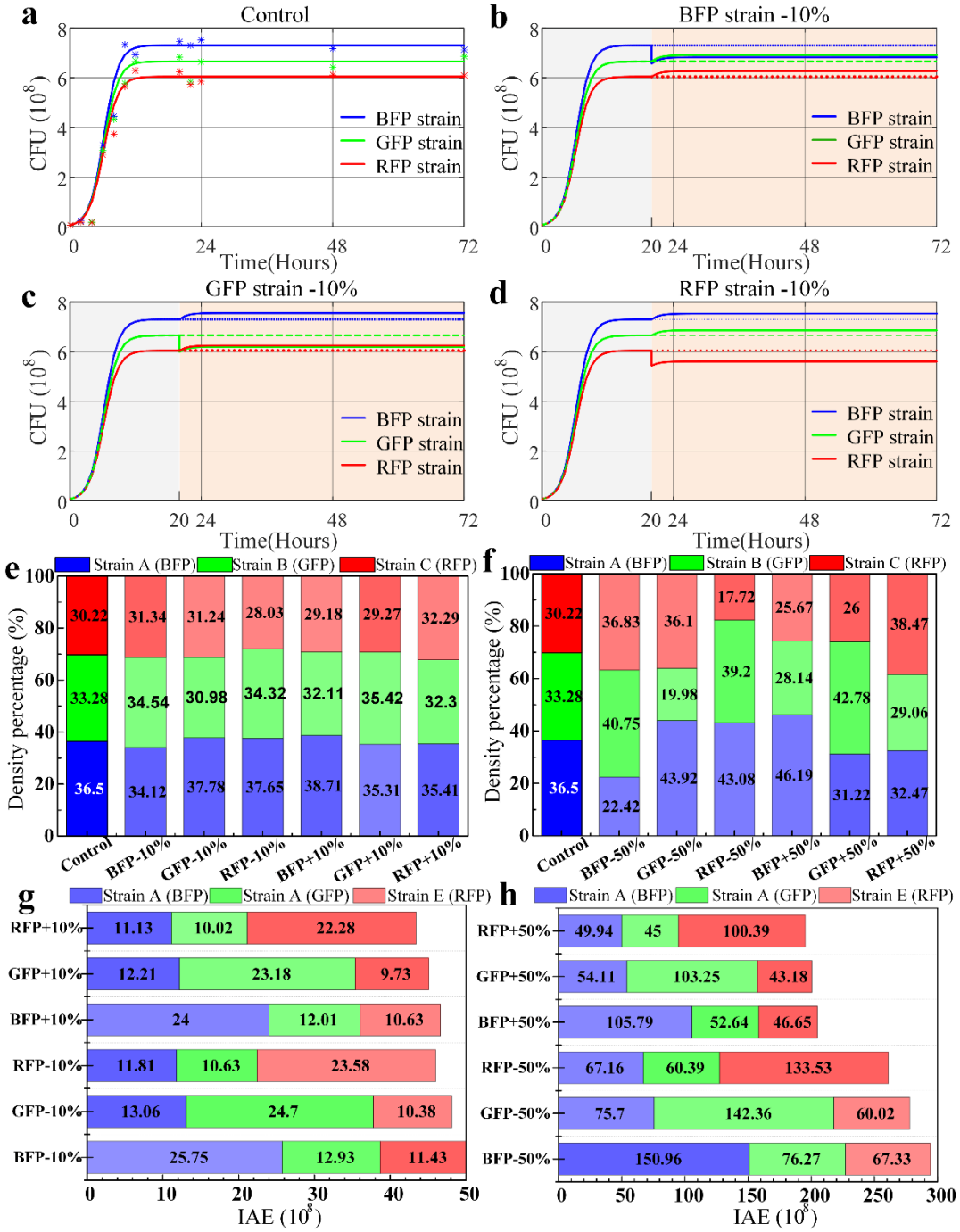

Supplementary Fig. 9. Modelling results for the circular microbiota with different disturbances imposed on strain A (BFP strain), strain B (GFP strain), or strain E (RFP strain). a. Cell growth obtained from modelling (lines) and experiments (stars). The experimental results are from the control of circular-interaction consortium shown in Fig. 4b. b-d. Responses of cell densities to -10% disturbances of each strain in the consortium; e-f. Cell density percentages of each strain under different disturbances; g-h. IAE (ranging from 20 h to 72 h) under different external disturbances.

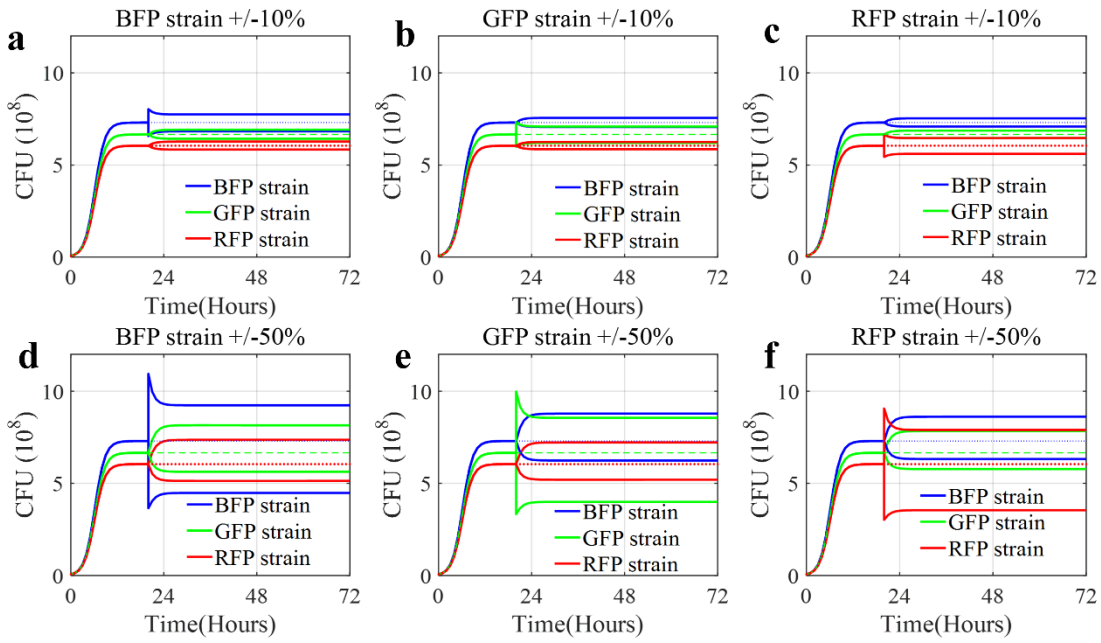

Supplementary Fig. 10. Simulation results for the circular microbiota with ±10% or ±50% disturbance imposed on strain A (BFP strain), strain B (GFP strain), or strain E (RFP strain).

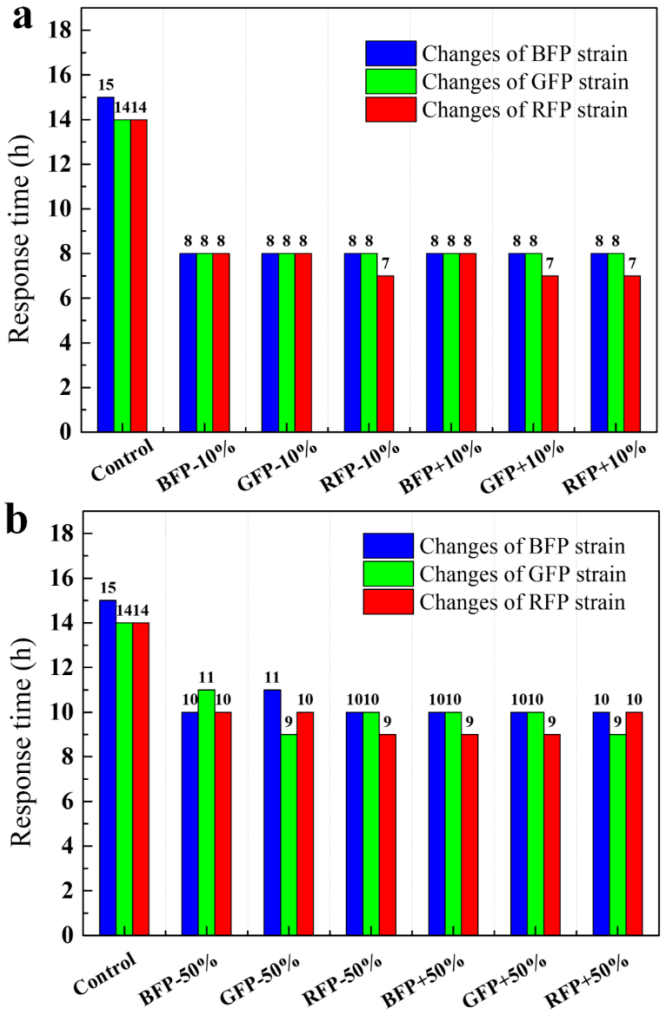

Supplementary Fig. 11. RT for the circular microbiota with ±10% or ±50% disturbance on strain A (BFP strain), strain B (GFP strain), or strain E (RFP strain).

Supplementary Table 8. Simulation results of RT and IAE for the circular microbiota with ±10% or ±50% disturbance.

Disturbances	Items	BFP strain	GFP strain	RFP strain
Control	RT (h)	15	14	14
	Population percentage (%)	36.50	33.28	30.22
BFP -10%	RT (h)	8	8	8
	IAE	25.75	12.93	11.43
	Population percentage (%)	34.12	34.54	31.34
GFP -10%	RT (h)	8	8	8
	IAE	13.06	24.7	10.38
	Population percentage (%)	37.78	30.98	31.24
RFP -10%	RT (h)	8	8	7
	IAE	11.81	10.63	23.58
	Population percentage (%)	37.65	34.32	28.03
BFP +10%	RT (h)	8	8	8
	IAE	24	12.01	10.63
	Population percentage (%)	38.71	32.11	29.18
GFP +10%	RT (h)	8	8	8
	IAE	12.21	23.18	9.73
	Population percentage (%)	35.31	35.42	29.27
RFP +10%	RT (h)	8	8	7
	IAE	11.13	10.02	22.28
	Population percentage (%)	35.41	32.3	32.29
BFP -50%	RT (h)	10	11	10
	IAE	150.96	76.27	67.33
	Population percentage (%)	22.42	40.75	36.83
GFP -50%	RT (h)	11	9	10
	IAE	75.7	142.36	60.02
	Population percentage (%)	43.92	19.98	36.1
RFP -50%	RT (h)	10	10	9
	IAE	67.16	60.39	133.53
	Population percentage (%)	43.08	39.2	17.72
BFP +50%	RT (h)	10	10	9
	IAE	105.79	52.64	46.65
	Population percentage (%)	46.19	28.14	25.67
GFP +50%	RT (h)	10	10	9
	IAE	54.11	103.25	43.18
	Population percentage (%)	31.22	42.78	26
RFP +50%	RT (h)	10	9	10
	IAE	49.94	45	100.39
	Population percentage (%)	32.47	29.06	38.47

3.3 Topology optimization for the one-way QS signal transmission

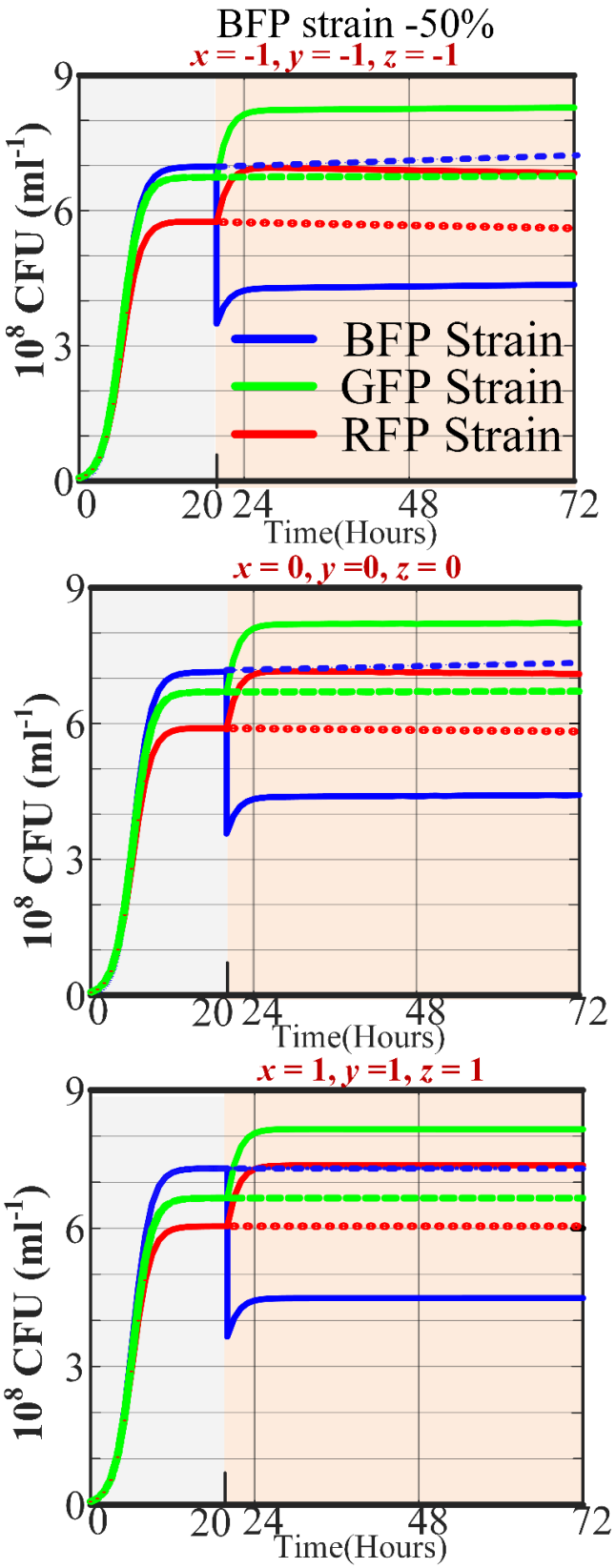

Supplementary Fig. 12. Time evolution of cell densities in the consortium with a topology configuration (x,y,z) of (-1,-1,-1), (0,0,0) and (1,1,1).

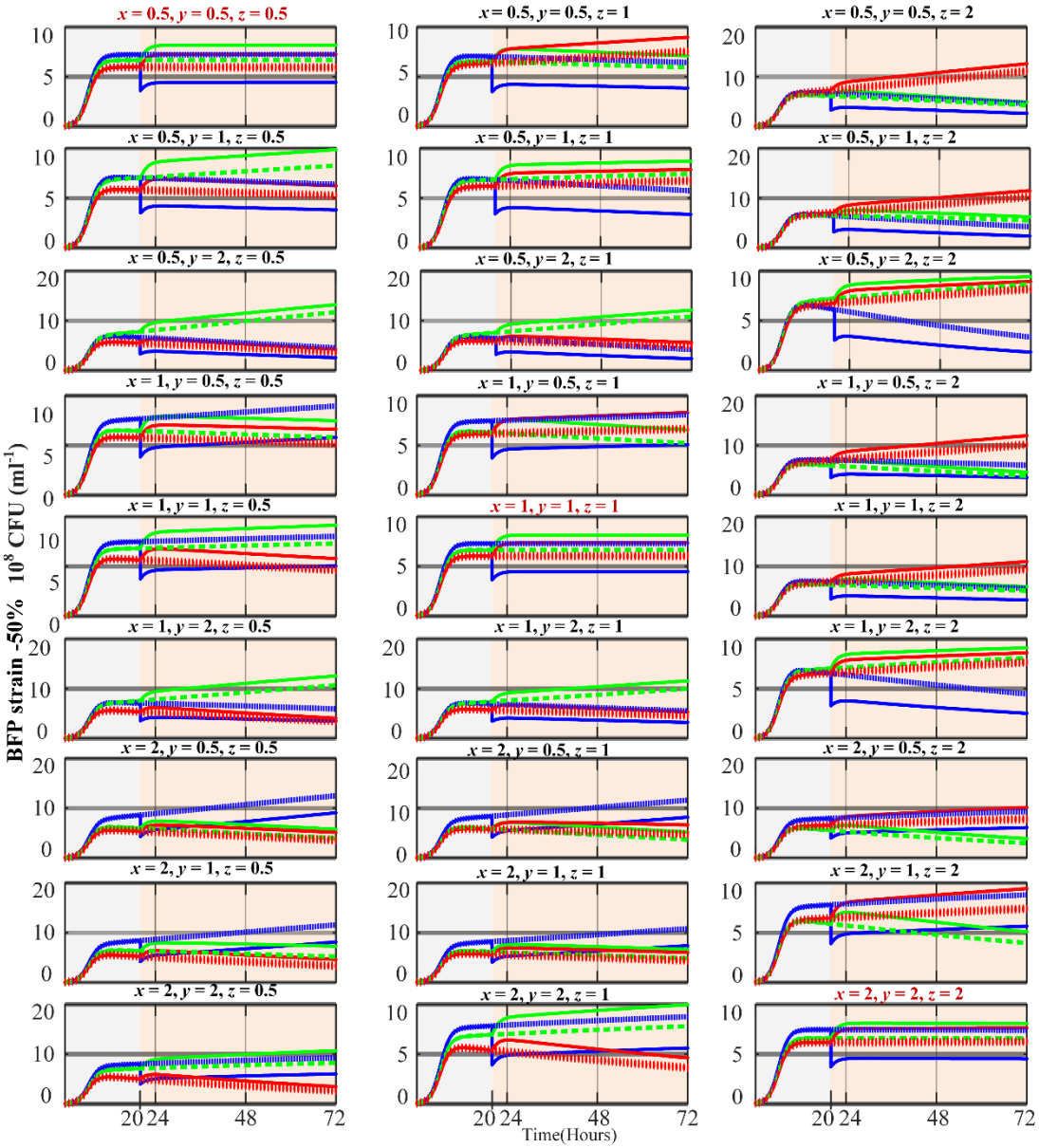

Supplementary Fig. 13. Time evolution of cell densities in the consortium with tunable x, y and z whose values can be chosen among 0.5, 1, or 2.

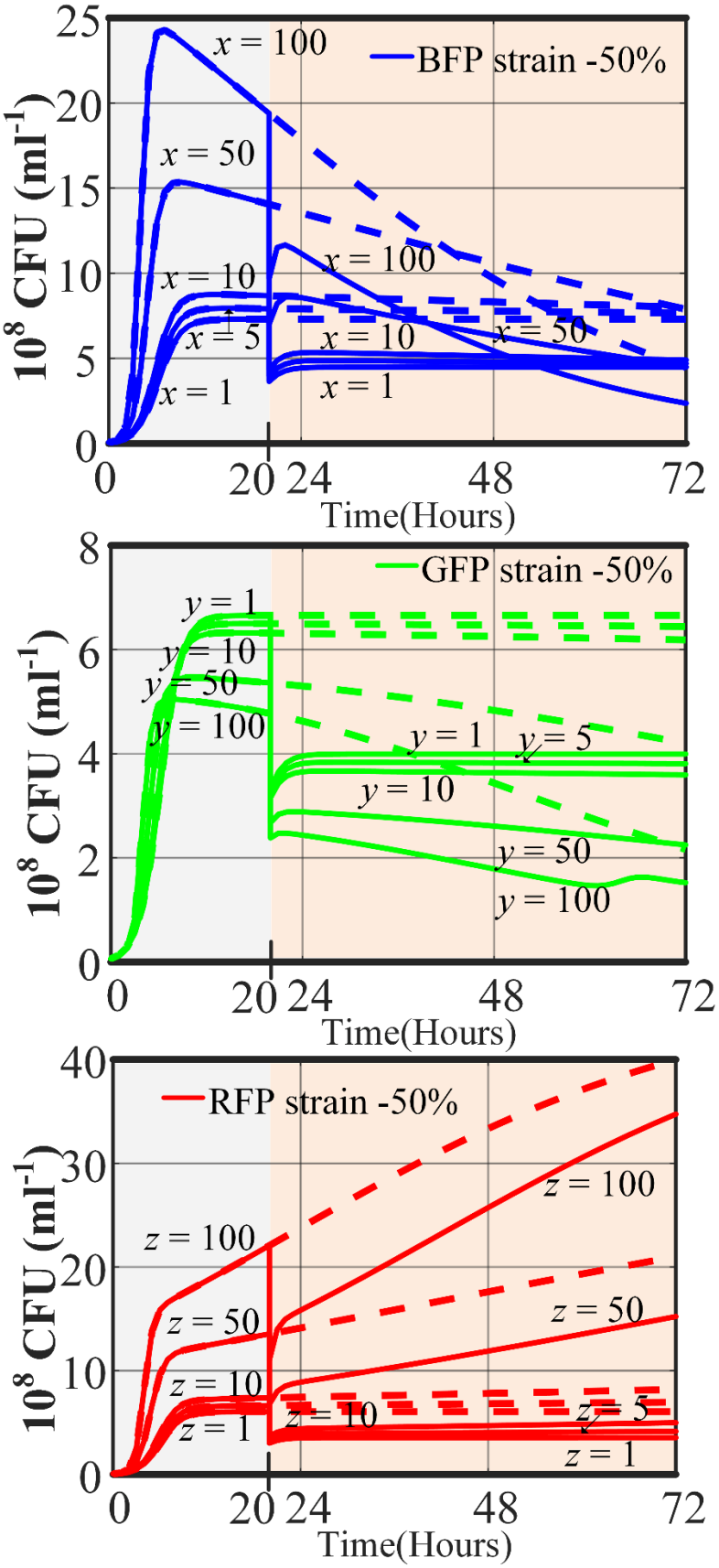

Supplementary Fig. 14. Sensitivity analysis of different promotion intensity on the dynamics of microbiota with different external disturbances

3.4 Analysis of operating conditions for the circular transmission

As three strains in the consortium will compete on space and nutrition, which will depend on the relative concentrations of strain cells, controlling of operation conditions like dilution rate (D) will be very important for the control of the consortium. Therefore, we conducted an analysis for D (being 0.01, 0.05, 0.076, 0.1, 0.134, or 0.3) on the cell growth of strains E, A, and B. As expected, cell densities decrease with the increase of D (Supplementary Fig. 15a-c). This indicates that it is difficult for the consortium to converge to another stable state by simply changing D.

We then conducted a sensitivity analysis for two operating parameters, the promoted cell growth rate ($x \cdot \gamma$) and D, which are both set in the range from 0.01 to 0.3. Supplementary Fig. 15d and 15e show the influential map of the two parameters on the minimal fermentation time (MT) and response time (RT), respectively. We can see that MT and RT of the BFP strain increase with D. This is because that the competition among three strains is alleviated to a certain degree when the culture medium is diluted, so more cells can grow to reach the condition where the competition becomes intense again. In addition, higher D would lead to a higher dilution rate of QS signal molecules, thus weakens the signal transmission. Interestingly, the obtained influential maps show that MT and RT reach a minimum when D and the promoted cell growth rate are approximately equal. Therefore, there is a need for the simultaneous optimization of D and the promoted cell growth rate to get a relatively short MT and RT.

In addition, we also tested the sensitivity of the consortium dynamics on the initial inoculation ratio of three strains. The results show that MT and RT of strain A, strain B, and strain E were almost equal for different initial inoculation ratios (Supplementary Fig. 15f, 15g, and 16), suggesting that when one of the strains reaches a stable state, the other two strains would be in a stable state shortly. In general, the more uneven the initial inoculation ratio is, the longer time for the system to reach a stable state (Supplementary Fig. 15f). For example, the cases with two initial ratios of strain A, B, and E (1:5:5 and 1:5:10) had a much longer MT (about 180 h) and RT (about 220 h), which was due to the much less cell density of strain A (BFP strain). Furthermore, for the two cases of 1:5:5 and 1:5:10, different disturbances also affect RT values with the order of RT for A disturbance > RT for E disturbance > RT for B disturbance (Supplementary Fig. 16).

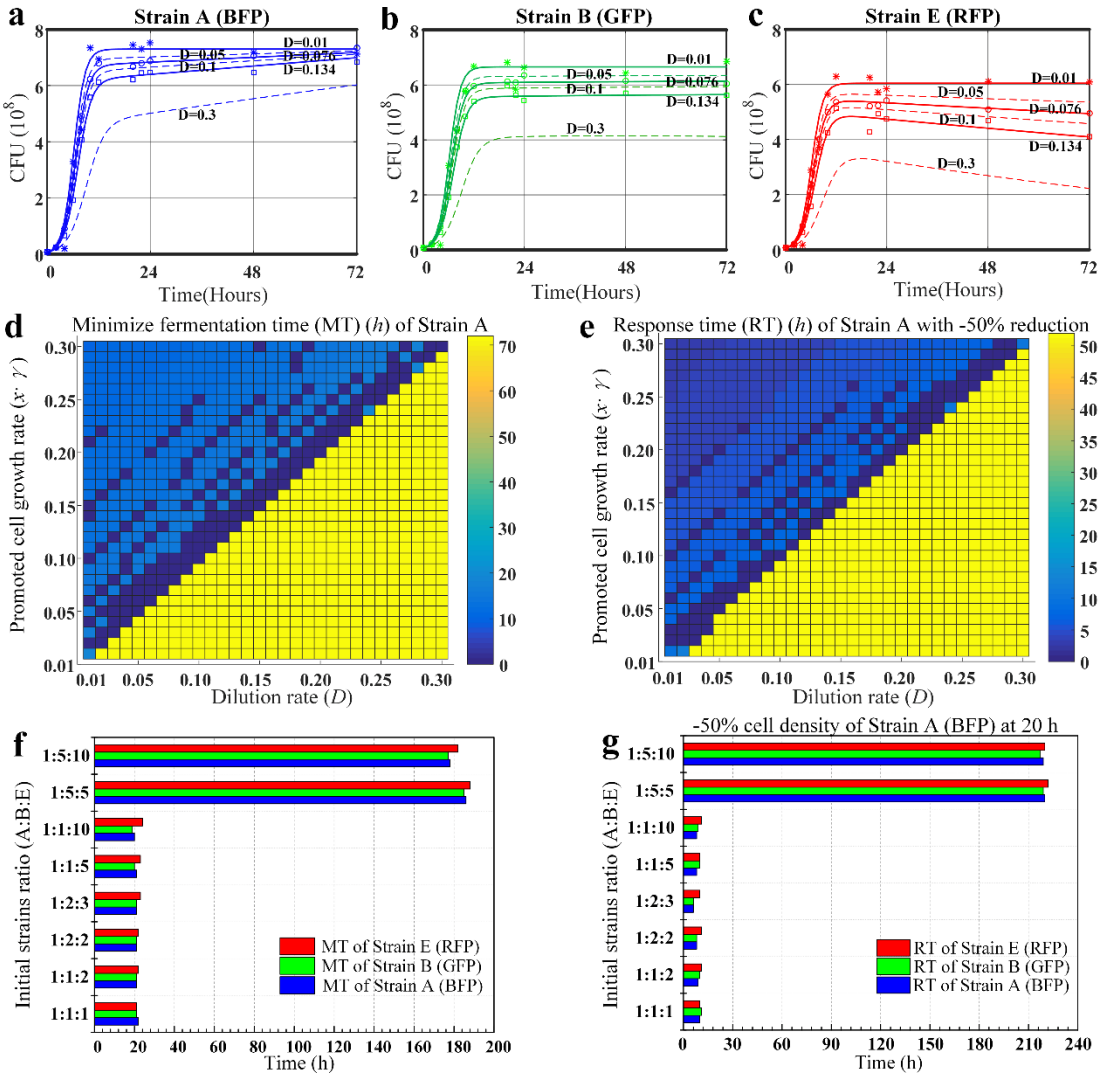

Supplementary Fig. 15. Dynamic responses of the circular consortium to various operating conditions. a-c. Growth curves of strain A, B, and E obtained from modelling (lines and dash lines) and experiments (stars, circles, and squares) with different dilution rate (*D*). d-e. Sensitivity analysis results of the MT and RT of BFP strain with or without -50% cell density disturbance for various combinations of the promoted cell growth rate ($x^*\gamma$) and *D*. Note that the smaller the value represented by the color (blue), the faster BFP strain can reach a stable state. f-g. Results of MT and RT of BFP, GFP, and RFP strains for different initial inoculation ratios (Strain A:Strain B:Strain E, A:B:E). The total cell density was set to be 0.2 (10^8 CFU ml^{-1}).

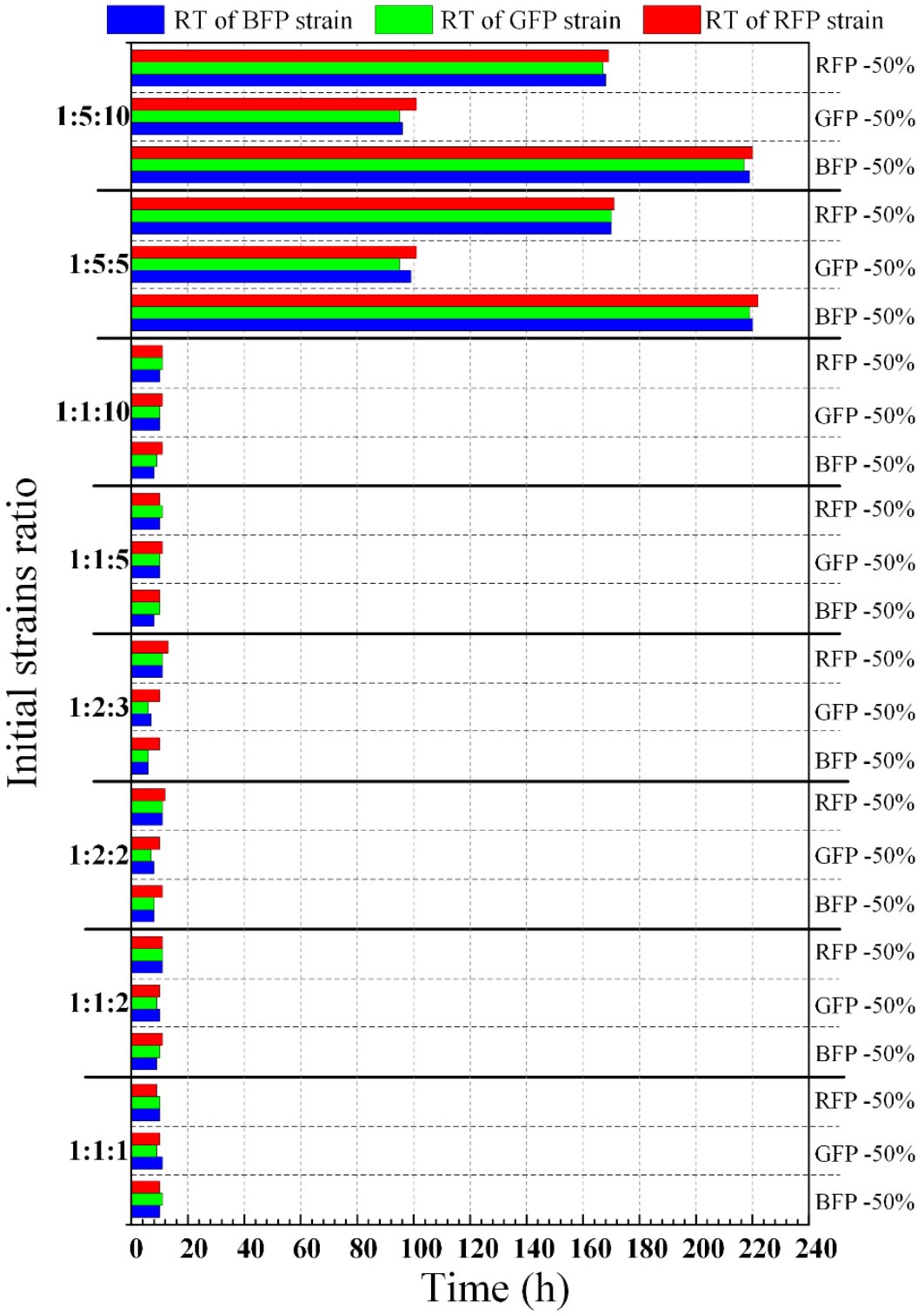

Supplementary Fig. 16. RTs obtained under various initial inoculation ratios and different external disturbances.

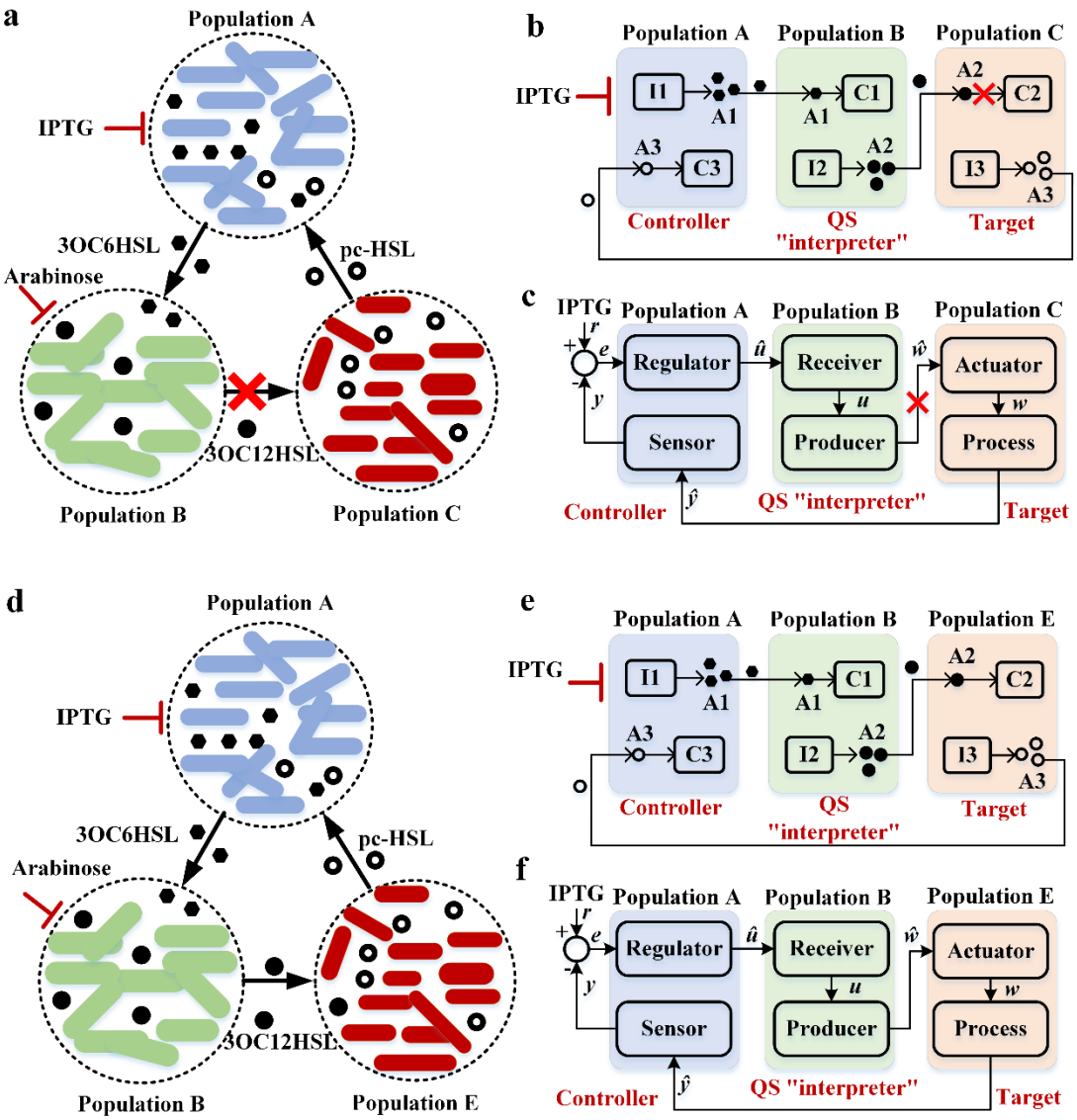

Supplementary Fig. 17. Control structure of the linear and circular QSCN. a. Schematic diagram of a QS-based consortium with a linear interaction pattern of C→A→B based on pc-HSL and 3OC6HSL. b. Simplified QS signals transmission among "Controller", QS "interpreter", and "Target" for the linear QSCN. c. When adding IPTG, "Controller" contained the regulator for providing inputs ($\hat{u}$) to the QS "interpreter" (including receiver and producer) and sensor for retrieving information ($\hat{y}$) on the process status in the Target (strain C), which cannot communicate with strain B. d. Schematic diagram of a consortium with a circular interaction of pattern E→A→B→E based on pc-HSL, 3OC6HSL, and 3OC12HSL. e. Simplified QS signals transmission among "Controller", QS "interpreter", and "Target" for the circular QSCN. f. When adding IPTG, "Controller" contained the regulator for providing inputs ($\hat{u}$) to the QS "interpreter" (including receiver and producer) that sending control information ($\hat{w}$) to Target (strain E), and sensor for retrieving information ($\hat{y}$) on the process status in the Target (strain E) according to the control error e computed by the comparator as the difference between the reference r and the measured output y.

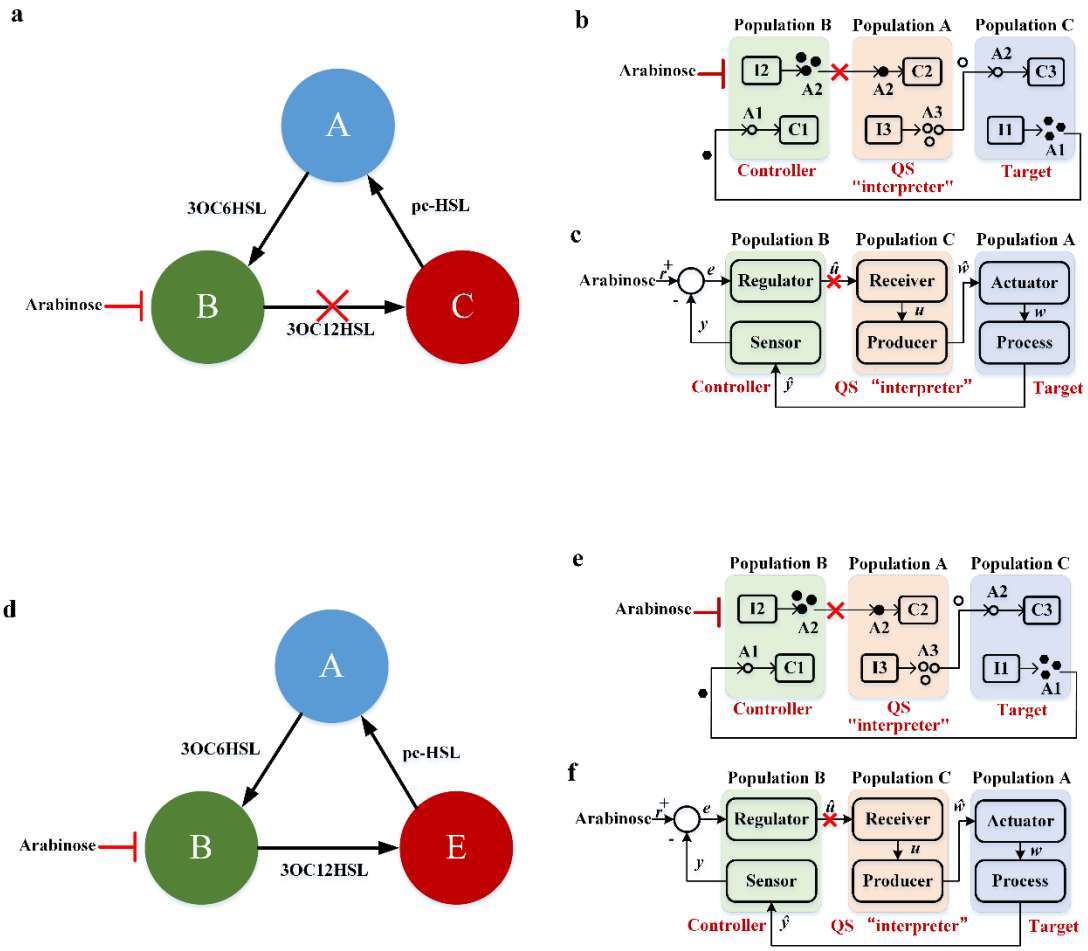

Supplementary Fig. 18. Control structure of the linear and circular QSCN. a. Schematic diagram of a QS-based consortium with a linear interaction pattern of C→A→B based on pc-HSL and 3OC6HSL. b. Simplified QS signals transmission among "Controller", QS "interpreter", and "Target" for the linear QSCN. c. When adding arabinose, "Controller" contained the regulator for providing inputs ($\hat{u}$) to the QS "interpreter" (including receiver and producer) and sensor for retrieving information ($\hat{y}$) on the process status in the Target (strain C), which cannot communicate with strain B. d. Schematic diagram of a consortium with a circular interaction of pattern E→A→B→E based on pc-HSL, 3OC6HSL, and 3OC12HSL. e. Simplified QS signals transmission among "Controller", QS "interpreter", and "Target" for the circular QSCN. f. When adding arabinose, "Controller" contained the regulator for providing inputs ($\hat{u}$) to the QS "interpreter" (including receiver and producer) that sending control information ($\hat{w}$) to Target (strain E), and sensor for retrieving information ($\hat{y}$) on the process status in the Target (strain E) according to the control error e computed by the comparator as the difference between the reference r and the measured output y.

4. References

1. Gu F*, et al.* Quorum sensing-based dual-function switch and its application in solving two key metabolic engineering problems. *Acs. Synth. Biol.* **9**, 209-217 (2020).
2. Liu J*, et al.* Two-stage carbon distribution and cofactor generation for improving l-threonine production of escherichia coli. *Biotechnol. Bioeng.* **116**, 110-120 (2019).
3. Miller MB, Bassler BL. Quorum sensing in bacteria. *Annu. Rev. Microbiol.* **55**, 165-199 (2001).
4. Sandoz KM, Mitzimberg SM, Schuster M. Social cheating in pseudomonas aeruginosa quorum sensing. *Proc. Natl Acad. Sci. USA* **104**, 15876-15881 (2007).
5. Scott SR, Din MO, Bittihn P, Xiong L, Tsimring LS, Hasty J. A stabilized microbial ecosystem of self-limiting bacteria using synthetic quorum-regulated lysis. *Nat. Microbiol.* **2**, 17083 (2017).
6. Wu S*, et al.* Combinational quorum sensing devices for dynamic control in cross-feeding cocultivation. *Metab. Eng.* **67**, 186-197 (2021).
7. Balagadde FK*, et al.* A synthetic escherichia coli predator-prey ecosystem. *Mol. Syst. Biol.* **4**, 187-195 (2008).
8. Song H, Payne S, Gray M, You L. Spatiotemporal modulation of biodiversity in a synthetic chemical-mediated ecosystem. *Nat. Chem. Biol.* **5**, 929-935 (2009).
9. Scott SR, Hasty J. Quorum sensing communication modules for microbial consortia. *Acs. Synth. Biol.* **5**, 969-977 (2016).
10. Kylilis N, Tuza ZA, Stan GB, Polizzi KM. Tools for engineering coordinated system behaviour in synthetic microbial consortia. *Nat. Commun.* **9**, 2677 (2018).
11. Wu S, Qiao J, Yang A, Liu C. Potential of orthogonal and cross-talk quorum sensing for dynamic regulation in cocultivation. *Chem. Eng. J.*, 136720 (2022).
12. Subhayu Basu, Yoram Gerchman, Cynthia H. Collins, Arnold FH, Weiss R. A synthetic multicellular system for programmed pattern formation. *Nature* **434**, 1130-1134 (2005).
13. Wu S, Guo K, Liu C, Qi W, Zhang T, Liu H. Design and control for a dividing-wall column with a partial condenser for pretreating an industrial multi-component reformed gasoline mixture. *The Canadian Journal of Chemical Engineering* **96**, 2431-2442 (2018).